Published in final edited form as:
Acta Biomater. 2012 May ; 8(5): 1939–1947. doi:10.1016/j.actbio.2012.01.033.

In vitro studies on the effect of particle size on macrophage responses to nanodiamond wear debris

Vinoy Thomas[a], **Brian A. Halloran**[b], **Namasivayam Ambalavanan**[b], **Shane A. Catledge**[a], and **Yogesh K. Vohra**[a,*]

[a]Center for Nanoscale Materials and Biointegration (CNMB), Department of Physics, College of Arts and Sciences, University of Alabama at Birmingham (UAB), Birmingham, AL 35294, USA

[b]Department of Pediatrics, Division of Neonatology, School of Medicine, University of Alabama at Birmingham (UAB), Birmingham, AL 35294, USA

Abstract

Nanostructured diamond coatings improve the smoothness and wear characteristics of the metallic component of total hip replacements and increase the longevity of these implants, but the effect of nanodiamond wear debris on macrophages needs to be determined to estimate the long-term inflammatory effects of wear debris. The objective was to investigate the effect of the size of synthetic nanodiamond particles on macrophage proliferation (BrdU incorporation), apoptosis (Annexin-V flow cytometry), metabolic activity (WST-1 assay) and inflammatory cytokine production (qPCR). RAW 264.7 macrophages were exposed to varying sizes (6, 60, 100, 250 and 500 nm) and concentrations (0, 10, 50, 100 and 200 μg ml^{-1}) of synthetic nanodiamonds. We observed that cell proliferation but not metabolic activity was decreased with nanoparticle sizes of 6–100 nm at lower concentrations (50 μg ml^{-1}), and both cell proliferation and metabolic activity were significantly reduced with nanodiamond concentrations of 200 μg ml^{-1}. Flow cytometry indicated a significant reduction in cell viability due to necrosis irrespective of particle size. Nanodiamond exposure significantly reduced gene expression of tumor necrosis factor-α, interleukin-1β, chemokine Ccl2 and platelet-derived growth factor compared to serum-only controls or titanium oxide (anatase 8 nm) nanoparticles, with variable effects on chemokine Cxcl2 and vascular endothelial growth factor. In general, our study demonstrates a size and concentration dependence of macrophage responses in vitro to nanodiamond particles as possible wear debris from diamond-coated orthopedic joint implants.

Keywords

Diamond; Nanoparticles; Wear debris; Macrophage; Osteolysis

1. Introduction

Data from the American Academy of Orthopedic Surgeons show that more than 418,000 total and partial knee replacements and 328,000 total and partial hip replacements are performed in the US each year, and the number of total knee replacements and total hip replacements performed in the US is expected to leap by 673% and 174%, respectively, by the year 2030 [1]. Wear of articulating surfaces involving cobalt–chromium–molybdenum (CoCrMo) alloy against polyethylene (components in the majority of hip and knee implants)

*Corresponding author. Tel.: +1 205 934 6662; fax: +1 205 934 8042. ykvohra@uab.edu (Y.K. Vohra).

has been cited as a dominant factor limiting the long-term success of the implants [2,3]. Wearing and the resultant generation of wear debris particles can lead to mechanical instability, decreased joint mobility, increased pain, deleterious biological responses, osteolysis, and ultimately component loosening and implant failure [2–4]. Large debris pieces are normally sequestered by fibrous tissue, while small debris is phagocytosed by macrophages and monocytes, which may release cytokines that result in inflammation. The inflammation cascade also leads to the recruitment of activated osteoclasts at the bone–implant interface and to bone resorption around the implant. One solution for this problem of osteolysis caused by wear debris is to coat harder materials, such as diamond, on the articulating surfaces to improve wear resistance and to reduce the number and size of debris particles generated.

Studies have shown that less wear occurs with metal-on-metal hip prostheses, up to 100 times less than that of polyethylene-on-metal, and CoCrMo metal articulation results in smaller debris particles than metal-on-polyethylene articulation [5–7]. The CoCrMo debris from a metal-on-metal articulation were shown to be in the range of 6–744 nm, with an average size of 42 nm [6], whereas polyethylene particles ranged from 0.1 to 5 μm (100–5000 nm) [8]. As the metal wear-particles are relatively smaller than polyethylene particles, they may be less prone to inflammation and osteolytic reaction. A study investigating bone and tissue reactions to metal debris in several metal-on-metal components revealed that there were fewer macrophages and giant cells than typically seen in tissues around metal-on-polyethylene joints [2]. Unfortunately, there are concerns and debate associated with metal sensitivity and metallosis, the release of alloy constituents into the surrounding tissue. The term “metallosis” has also been used to describe the intraoperative findings of gross metallic debris and blackening of periprosthetic tissue [9]. Metal sensitivity, which affects approximately 10–15% of the general population, is much higher among patients with failed implants [10–12].

Nanostructured diamond (NSD) coatings or diamond-like carbon coatings have been shown to greatly enhance the wear resistance and to prevent leaching of metallic ions from orthopedic and dental implants into the body [13,14]. For example, NSD coatings improve the smoothness and wear characteristics of the femoral head component of total hip replacements, and hence minimize wear debris formation and increase implant longevity [14–16]. NSD coatings developed in our laboratory have shown promise as potential wear-resistant coatings on Ti–6Al–4V for use in temporomandibular joint prostheses [16–18] and on CoC-rMo for hip joint prostheses [19]. However; the brittleness/delamination of a thin diamond coating may lead to the formation of wear-debris of nanodiamonds from diamond-on-diamond and diamond-on-polyethylene couples.

The average particle size of diamond-on-diamond debris is expected to be considerably smaller than polyethylene debris, due to the increased material hardness. In addition, hip simulator studies [20] involving diamond–diamond couples have shown very marked reduction in wear debris volume ($<10^{-4}$ mm^3 $year^{-1}$), compared to first-generation CoCrMo–CoCrMo couples (1–5 mm^3 $year^{-1}$) and to polyethylene couples (50–100 mm^3 $year^{-1}$). The reduced wear volume and particle size expected for diamond articulation is a major advantage over conventional orthopedic bearings. However, a very low wear volume itself is not the only key factor governing the long-term clinical outcome of a total joint replacement. The number, size, or morphology and biological response to wear particles released are also important factors. In addition, there exists considerable discussion over the possible distribution of these smaller nanoparticles in the body, and their biological effects on cells and tissues. The objective of this study was to evaluate systematically the response of inflammatory cells, macrophages, to synthetic nanodiamond particles of various sizes as potential wear debris from diamond-on-diamond couples. Recently, synthetic nanodiamond

particles have attracted much attention in therapeutic delivery and bio-imaging applications due to their innate inertness and emission of fluorescence from nitrogen vacancies (N-V color centers) [21–25]. A few studies have reported the cytocompatibility of nanodiamond particles (2–10 nm), produced by an explosive detonation technique, from the standpoint of cell viability using the MTT assay, ATP production and ROS measurement with different cell types in vitro [26,27,23]. An in vivo study to investigate the fate of nanodiamonds (50 nm diameter) in mice has shown accumulation of 60% of injected particles in the liver after 0.5 h of post-dosing and the rest in the spleen and lung [28]. However, the effect of the size and concentration of nanodiamond particles when exposed to phagocytes such as macrophages and their potential activation from a standpoint of bone resorption/implant failure has not yet been explored in detail.

An ongoing concern in conventional total joint replacement prostheses is osteolysis and aseptic loosening induced by wear-debris originating from the interfaces of articulating components [29–32]. Macrophages and multinuclear giant cells (MNGCs, formed by the fusion of macrophages) are the primary scavengers of wear particles and their response appears to depend on the nature, size and concentration of the particles accumulated [3,4]. Poly-ethylene debris surrounded by macrophages and phagocytosis of debris by macrophages was frequently observed at the interface tissues [33]. Phagocytic cells engulf wear debris and become activated, releasing pro-inflammatory cytokines, degradative enzymes and other factors that stimulate osteoclasts [33–35]. For a diamond-on-polyethylene couple, polyethylene has much lower hardness compared to diamond and would account for essentially all of the wear-particles generated. However, for a diamond-on-diamond couple, diamond wear-particles are expected to be produced, and the effects of these particles on inflammatory cells must be evaluated. A limitation is that the amount of nanodiamond debris generated from a wear couple in a simulator is expected to be negligible due to its superior hardness, smoothness and wear-resistant properties [16,36]. Moreover, the particles produced in simulators or by other means do not consistently resemble wear debris particles from joint implants in vivo [37]. Therefore, synthetic nanodiamond particles of different sizes (6–500 nm) and varying concentrations (10–200 μg ml^{-1}) were utilized to interact with macrophage cells in the present study. Macrophage response to titanium dioxide (anatase) particles (~8 nm average size), a well-known nanoparticle, was evaluated for the purpose of comparison.

2. Materials and methods

2.1. Materials

Two types of synthetic nanodiamond particles were used in this study: (1) explosion synthesized nanodiamond (detonation nanodiamonds having particles of 2–10 nm) with average particle size of 6 nm, surface area of 283 m^2 g^{-1}, and purity of 98% (from Nanostructured and Amorphous Materials, Inc., TX), and (2) high-pressure high-temperature milled nanodiamonds (10 cts MA4 Diamond Powder from Hyprez-Engis Inc., IL) with an average particle size of 60 nm (Hyprez 0.0–0.10 μm), 100 nm (Hyprez 0.0–0.20 μm), 250 nm (Hyprez 0.0–0.50 μm) and 500 nm (Hyprez 0.0–1 μm) and a purity of 98%. The particle shape and purity were in conformance with ANSI standards B74.20-2004 (micron sizes) or B74.16-2002 (sieve sizes) as certified by the manufacturer. Nanodiamond particles were further purified by acid treatment using 9:1 sulfuric acid/nitric acid [38]. Anatase (TiO_2) particles were also commercially obtained to use as a comparison agent. Thus, the dispersion of nanodiamond particles in phosphate-buffered saline (PBS) could be readily achieved via sonication.

RAW 264.7 murine macrophages (ATCC TIB-71; Manassas, VA) cultured in vitro [39,26,23] in DMEM with 10% fetal calf serum (FCS) with penicillin–streptomycin at 5% CO_2, 37 °C were used to evaluate their responses to nanodiamond particles.

2.2. Characterization of nanodiamond particles

Raman spectra were acquired using a Dilor *x-y* spectrometer using excitation from the Coherent argon ion laser line output at 514.5 nm and laser power of 100 mW, focused to a spot size of 1 μm. The Raman scattered signal was analyzed by a high-resolution spectrometer (1 cm^{-1} resolution) coupled to a CCD detector.

X-ray diffraction (XRD) patterns were measured using a thin film diffractometer (X'pert MPD, Philips, Eindhoven, The Netherlands) with Cu anode (λ = 0.154154 nm), generator voltage of 45 kV, tube current of 40 kA, and glancing angle of 3°. The step size was 0.04° and time per step was 3 s.

Fourier transform infrared (FT-IR) spectra were recorded using an IR spectrophotometer (ThermoFisher Co., USA). The nanodiamond powders were scanned in attentuated total reflectance mode and the spectra were obtained with 64 scans per sample in the range from 4000 to 400 cm^{-1}.

Characterization of the size and morphology of nanoparticles was also performed by transmission electron microscopy (TEM) imaging using a FEI Tecnai T12 microscope at 80 kV acceleration voltage. To prepare the samples of nanoparticles for TEM studies, a drop of dilute aqueous solution of nanodiamond or TiO_2 was deposited and dried on TEM copper grid that had first been covered with a thin film of Formvar-supported carbon.

2.3. Preparation of nanodiamond solutions

Stock solutions of nanodiamonds were prepared at concentration of 20 mg ml^{-1} in PBS and dispersed well in the medium by sonication for 15 min using a Microson Ultrasonic Cell Disruptor equipped with a CM-1 Converter micro tip (Heat Systems Ultrasonic Inc., Farmingdale, NY) at 80% power. Solutions were then autoclaved for 15 min at 121 °C and 15 psi to sterilize them. Nanodiamond solutions of different concentrations ranging from 10 to 200 μg ml^{-1} were prepared from the stock solution and ultrasonicated further using a bath sonicator for 15 min before exposing them to cells.

2.4. Cell proliferation and metabolic activity studies

Cell proliferation and metabolic activity studies in the presence of varying concentrations (10–200 μg ml^{-1}) of nanodiamond particles were assayed by BrdU (cell proliferation; MBL International, Woburn, MA) and WST-1 (metabolic activity; Quick Cell Proliferation Assay Kit (MBL Int., Woburn, MA) assays, as indicated by the manufacturer. Nanodiamonds were incubated with 10% human serum at 4 °C overnight and then plated with ~40,000 Raw 264.7 cells/well on 96-well plates. After incubation for 24 h, WST-1 reagent was added for 60 min prior to reading supernatants at $OD_{450\ nm}$ or cells were incubated with BrdU labeling reagent 120 min prior to BrdU assay.

To evaluate the effect of higher serum protein content on macrophage responses, nanodiamonds (50 μg ml^{-1}) were incubated with 30% human serum at 4 °C overnight and then plated with ~40,000 Raw 264.7 cells/well in fetal calf serum (FCS)-free MEM (Serum-free medium) or MEM containing 10% FCS, on 96-well plates, followed by WST-1 or BrdU assay.

2.5. Apoptosis assay, flow cytometry and TEM imaging

Nanodiamonds were incubated with 10% human serum at 4 °C overnight and then plated with Raw 264.7 cells in MEM containing 10% FCS, on 24-well plates, at 200,000 cells per well with 50 μg ml^{-1} nanodiamonds. After incubation for 24 h, cells were lifted, washed with 250 μl PBS, and resuspended in binding buffer containing 1:100 propidium iodide and Annexin V-FITC (Annexin V-FITC Apoptosis Detection Kit, MBL International, Woburn, MA). Cells were analyzed using a Beckman Coulter Quanta SC Flow Cytometer. Annexin V-FITC labeled cells were plotted as early apoptotic cells and both propidium iodide + Annexin-V-FITC labeled cells were plotted as late apoptotic cells. Unlabeled (non-apoptotic or non-necrotic and) cells were plotted to quantify the cell viability.

For TEM imaging of phagocytosis of nanodiamond particles by macrophages, 50 μg ml^{-1} nanodiamonds (preincubated in 10% human serum) were added to 250,000 cells and plated onto 0.4 μm polycarbonate membranes (Costar 3407 Snapwell Permeable Supports, Corning Inc., Corning, NY) for 24 h at 37 °C in complete media. After fixation, dehydration and embedding in epoxy resin, TEM images were taken using a FEI Tecnai T12 Spirit transmission electron microscope.

2.6. Quantitative PCR analysis and ELISA

Nanodiamonds were incubated with 30% human serum at 4 °C overnight and then plated on a 24-well plate in triplicate at 50 μg ml^{-1} with 175,000 Raw 264.7 cells per well in complete media. After 24 h incubation, cells were washed twice with PBS and RNA was isolated using Trizol (Invitrogen, Carlsbad, CA). The protocol was followed according to the manufacturer's specifications [40]. RNA was purified using Ambion's RNAqueous Micro Kit (Ambion, Austin, TX). Reverse transcription (RT) into cDNA for RT-polymerase chain reaction (PCR) was performed using Ambion's Retroscript Kit. Quantitative PCR analysis was done using Applied Biosystems SYBR Green PCR Master Mix with a Biorad iCy-cler PCR Detection System. Primers for various cytokines and chemokines known to be involved in the macrophage activation and inflammation were designed [41] and are given in Table 1. The relative expression of the genes of interest was determined following normalization to the levels of housekeeping gene, 18S. The protein concentrations of representative cytokines (tumor necrosis factor (TNF)-α, interleukin (IL)-1β)) and cytokine (monocyte chemotactic protein (MCP-1)) in the case of 60 nm nanodiamond/macrophage exposure for 24 h were also evaluated by ELISA (Mouse Mix and Match Multi Analyte ELISA Kit, Qiagen, Valencia, CA).

2.7. Statistical analysis

Statistical analysis among groups was performed by analysis of variance (ANOVA). Multiple comparisons testing (Student–Newman–Keuls) was performed if statistical significance ($P < 0.05$) was noted by one-way ANOVA. For mRNA analysis, normalization was done by considering the average of the measurements (mRNA for gene of interest/18S RNA) in the PBS group as 1.0. Data are shown as means ± standard errors (SE).

3. Results and discussion

3.1. Characterization of nanodiamond particles

Synthetic nanodiamond particles of different sizes ranging from 6 to 500 nm were characterized by TEM, XRD, Raman and FT-IR spectroscopy (Figs. 1 and 2) to illustrate the chemical nature and purity of the materials. The existence of sp^2 and sp^3 carbons and important surface functional groups were evident from XRD, Raman and IR spectra. The Raman peak around 1332 cm^{-1} represents clear evidence of the presence of a diamond phase (sp^3) in the samples. Nanodiamonds oxidized by strong acid exhibit many surface

bound –OH and –COOH functional groups, as observed in the FT-IR spectra (Fig. 2). A strong absorption at 3420 cm^{-1} and medium-intensity shoulder peaks in the 2800–3000 cm^{-1} region were attributed to the presence of O–H or N–H and C–H groups, respectively (not shown in Fig. 2), and peaks around 1800 cm^{-1} and the band between 1750 and 1740 cm^{-1} were due to the C=O of the anhydride and carboxylic acid group, respectively. Other bands around 1631, 1450, 1330 1250 and 1100 cm^{-1} are attributed to C=C, and to C–O stretching and bending deformation modes of carboxylic acid, and the anhydride, carbonyl, NH, CH and C=C surface functional groups in oxidized diamonds. It is clear that introduction of more –COOH groups in the nanodiamonds not only renders them dispersed well in PBS (especially at lower concentrations), but also provide strong affinities towards serum proteins as reported elsewhere [38]. The strong protein-binding affinity is attributed to the interplay of various interactions (ionic interactions, van der Waals interactions, hydrogen bonding and hydrophobic interaction) between proteins and surface groups in nanodiamonds [42]. No crystalline or turbostratic graphitic carbon features could be observed in XRD spectra, except for 6 nm detonation particles. As the particle size increased from 6 to 500 nm, the nanodiamond crystallinity increased as indicated by the increase in intensity of the (111) peak. The mean primary particle size determined from the XRD data (using the Lorentzian fitting of the 111 peak in the XRD spectrum and the Scherrer equation) confirmed the average particle size of nanodiamonds. For example, the calculated size for 6 nm particles was ~4 nm.

Representative TEM images of nanodiamond and TiO_2 particles (from a drop of dilute aqueous solution of nanoparticles deposited on TEM copper grid) are shown in Fig. 3. TEM images show that the particles are partly agglomerated with a relatively better dispersion of TiO_2 particles in aqueous medium due to the inherent hydrophilic oxide layer. TEM images indicate that the average size of the TiO_2 particles is ~8 nm.

3.2. Cytotoxicity and cell-proliferation studies

The morphology of macrophages in the presence of nanoparticles as shown in Fig. 4 illustrates that both cells with and without the addition of nanoparticles solutions grew normally, with no obvious differences in cell morphology. Upon attachment and growth, however, some of the cells developed elongated extensions and others remained round in PBS, in serum only, or in nanoparticle wells. Nanodiamond particles from the surrounding media agglomerated at cell borders and within the cells. Cells incubated with 250 and 500 nm particles had intense dark borders, indicating larger particle agglomerates.

The cytotoxicity or the proliferative capacity of macrophages when exposed to the nanodiamond particles was assayed by WST-1 assay and BrdU immunoassay. In Wst-1 assay, diamond particles (6 nm) at various concentrations ranging from 10 to 200 μg ml^{-1} were exposed to macrophage cells for three time points and the data are given in Fig. 5. As the concentrations increased, up to 100 μg ml^{-1}, there were no significant variation in the optical density (OD) of the formazan product formed from the reaction between WST-1 reagent and the mitochondrial dehydrogenase of metabolically active cells. However, a marked decrease in the OD can be observed in the case of 200 μg ml^{-1} solution as given in Fig. 5. This observation is in agreement with the results reported by other researchers. Previously, Schrand et al. [26] have also shown no significant reduction in MTT Formazan product up to a concentration of 100 μg ml^{-1} of nanodiamond particles by MTT assay using neoroblastoma and macrophage cells and reported that detonation nanodiamonds (2–10 nm) were non-cytotoxic to these cells. However, a 2-fold increase in nanodiamond concentration (200 μg ml^{-1}) led to signs of toxicity (reduction in metabolic activity) in our study. This effect was more pronounced in the case of particles of extremely small size (6 and 60 nm) rather than particles of higher size.

To further evaluate the effect of nanodiamond particle size on cytotoxicity or cell proliferation, nanodiamond particles of various sizes at a constant concentration (50 μg ml^{-1}) were exposed to macrophages and cultured for 24 h in both serum-free medium (SFM) and 10% serum medium. Thereafter the responses were quantified by WST-1 assay (Fig. 6) and BrdU assay (Fig. 7). There was no significant variation in cell number with increase in particle size among the samples containing various size nanodiamond particles and TiO_2 nanoparticles. However, the cell number in all nanoparticle containing wells showed an increase compared to controls (without nanoparticles) as reported elsewhere [26]. Supernatants of nanodiamonds alone (without cells) did not show any absorbance at $OD_{450\ nm}$, after background correction, thus ruling out the possible refringence properties of the diamond particles due to their emission.

BrdU assay for quantifying the cells that are actively replicating their DNA confirmed no variation in cell number in wells containing particles above 100 nm, but showed a decrease in cell number in wells with smaller particles (6, 60 and 100 nm) in comparison with 250 and 500 nm particles (Fig. 7). This could be due to the increased number of particles of reduced size at a constant concentration (50 μg ml^{-1}) and the huge surface area of nanoparticles when the size is reduced to 100 nm and below. In an in vitro study of the inhibition of growth of human epithelial carcinoma cell line (A431) and normal human keratinocyte cell line (HaCaT) with nanodiamond particles using MTT assay, Burleson et al. [27] correlated cell viability to the number of particles in medium. They concluded that nanodiamonds inhibited the proliferation of the A431 cell line in a dose- and time-dependent manner and the cytotoxic effects were higher in A431 as compared to HaCaT. Our results in the present study demonstrating the size-dependent effect of nanodiamond particles on cell proliferation are novel.

3.3. Cell viability—subtraction of apoptotic and necrotic cells

We have also extended the study by culturing macrophage cells exposed to 50 μg ml^{-1} nanodiamonds for 24 h and quantified the cellular subpopulations at various stages of apoptosis and necrosis using flow cytometry to further confirm the effect of nanodiamond particles on cell death/viability. All the nanoparticles, irrespective of size, significantly decreased cell viability as shown in Fig. 8. Compared to the control samples, there were 50–60% as many viable cells remaining when incubated with nanodiamond particles compared to 80% when incubated with controls. However, no significant variation in cell death was observed among the nanoparticles, perhaps due to agglomeration of particles, leading to a reduction in the effective number of particles. It is interesting to note that no cells, or only a very few, were positive for early apoptotic dye (Annexin-V-FITC labeled cells) in any of the samples compared to controls, but significant numbers of late apoptosis labeled cells (propidium iodide + Annexin-V-FITC labeled cells) were observed in all the nanodiamond samples (Fig. 8), which could be attributed to nanoparticle-mediated necrosis. It may be assumed that after 24 h incubation, cells that have ingested diamond particles may also have a deleterious effect on surrounding cells. Optical and TEM imaging results confirmed the phagocytosis of nanoparticles by macrophages. TEM images are shown in Fig. 9, demonstrating internalization of nanoparticles into macrophage vacuoles in the case of both TiO_2 and diamond particles. The response of macrophages to wear debris depends, as mentioned earlier, on the nature, size and concentration of the particles. Large polystyrene beads (~3.5 μm) were shown to cause primarily macrophage necrosis, while smaller (~0.5 μm) polystyrene beads caused primarily macrophage apoptosis [5]. Another study showed that 0.24 μm polyethylene particles mildly stimulated macrophages to generate bone-resorbing activity and inflammatory markers, while 0.45–1.71 μm particles greatly stimulated inflammatory markers. In flow cytometric experiments, we have not observed any variation in cell-death through apoptosis pathways due to the variation in size of the

nanodiamond particles. However, there was a marked effect on the viability of macrophage cells attributed to the nanoparticle-mediated necrosis compared to control samples. Irrespective of the size, these nanodiamond particles were internalized by the macrophage cells as evident from the TEM observations.

3.4. Cytokine gene expression studies by qPCR

In order to quantify the inflammatory response of the macrophages to nanoparticles, cytokines such as TNF-α, IL-1β, chemokines such as Cxcl2 or MIP-1α (macrophage inhibitory protein), Ccl2 or MCP-1 (monocyte chemotactic protein), and growth factors such as VEGF (vascular endothelial growth factor) and PDGF (platelet-derived growth factor) synthesized by the macrophage cells were measured using quantitative reverse transcription PCR; these experiments may be considered complementary to the measures of apoptosis/necrosis. We chose the 24 h incubation period to avoid variability in the early regulation of TNF-α (which has strong autocrine feedback signals) in an effort to measure a cellular steady state. The qPCR results given in Fig. 10 show that most of the cytokines were reduced in the presence of nanodiamonds. Measurement of cytokines by ELISA confirmed that MCP-1 was reduced on exposure to nanodiamonds (60 nm size at 50 μg ml^{-1} for 24 h) ($OD_{450–570\ nm}$ = 0.83 ± 0.07 vs. 0.56 ± 0.04 in control; P = 0.002), but no significant differences in TNF-α (0.91 ± 0.2 vs. 1.34 ± 0.24) or IL-1 β (too low to measure) were noted. This may possibly be due to the decrease in cell viability as shown by apoptosis assay. Since the cells are dead/dying, they are probably in no condition to make new cytokines. However, the situation could be different in vivo as cells may release cytokines from pre-formed stores and then die, and these released cytokines might attract fresh macrophages from nearby tissue or the blood circulation.

TNF-α and IL-1β are known bone-resorbing or osteolytic factors expressed by many cells such as macrophages, monocytes, osteoclasts, etc.; their concentrations are low in cells in the absence of exogenous stimuli but become synthesized de novo when the cell is activated [43]. Studies have shown that TNF-α stimulates the production of pro-inflammatory adhesion molecules and increases the differentiation and maturation of osteoclasts, resulting in bone resorption both in vitro and in vivo [44–47]. IL-1β is a pro-inflammatory and pro-wound-healing cytokine that activates lymphocytes, chemokines such as MCP-1, and osteolytic cytokines such as TNF-α and IL-6. TNF-α production has been implicated in inducing apoptosis of adherent macrophage on biomaterials [48]. Of relevance to the present work was the absence of increased gene expression of both bone-resorbing pro-inflammatory factors when exposed to nanodiamond wear particles of varying sizes at a concentration of 50 μg ml^{-1}. Huang et al. [23] have also reported no significant variation in the mRNA levels for three genes (TNFα, IL-6 and iNOS) on exposure to very small sized detonation nanodiamonds (2–8 nm) at a relatively low concentration of 30 μg ml^{-1}. The reduction observed in our studies could be due to concentration-dependent effects. A comparable in vitro study that involved culturing RAW 264.7 cell line with metal particles (stainless steel) for 24 h showed up-regulation of both TNF-α and IL-1β with a significant number of late apoptotic cells [39].

The chemokine MIP-1α is involved in chemotaxis and recruitment of monocytes and leukocytes during inflammation, while the chemokine MCP-1 recruits macrophage and stimulates murine FBGC fusion in vivo [49]. MCP-1 also stimulates IL-1 and IL-6 release from monocyte/macrophages. VEGF, a pro-angiogenic cytokine, and PDGF, a connective tissue mitogen, have been implicated in periprosthetic osteolysis and subsequent aseptic loosening of implants following total hip arthroplasty [50–52]. VEGF promotes blood vessel dilation and angiogenesis in the event of inflammation to promote wound healing in damaged tissue. Therefore, a reduction in, or absence of, up-regulated expression of pro-inflammatory chemokines and pro-wound-healing (VEGF) cytokine levels in the presence

of nanodiamond particles suggests no severe signs of inflammation-related processes (compared to serum-only control).

The clinical consequences of wear debris cover a broad spectrum from radiolucencies to massive osteolysis and implant failure. For this reason, the reduction of wear debris should be a primary goal of new-generation orthopedic joint implants. We have developed ultra-smooth nanodiamond coatings by chemical vapor deposition (CVD) on orthopedic-implant metals (on titanium alloy for TMJ and on cobalt chrome alloy for hip joint) [16,18,36,53,54] and on Nitinol for stent applications [55]. We have measured the hardness of our NSD coatings [17,53,54] and shown them to be significantly harder (40–90 GPa, depending on processing conditions) than other forms of carbon widely reported in the literature [56], including various amorphous variations of diamond-like carbon (DLC) (15–35 GPa). The NSD coatings are more resistant to scratching by third-body wear particles, such as bone cement, due to the high hardness and low surface roughness (rms value < 8 nm) of the coatings [16,17,53,54]. These NSD coatings are comprised of nanoscale diamond grains (<5 nm) within an amorphous carbon matrix, and have also shown excellent biocompatibility and corrosion resistance in physiological fluids [57,58]. However, the translational potential of these nanostructured coatings is in large part determined by their biocompatibility and bioperformance (wear-resistance of articulating surface and osteointegration of the rest). Although the failure or loosening of joint replacement components is often multifactorial [59], wear-debris induced osteolysis is a key factor among them. Macrophages activated by the phagocytosis of particulate wear-debris are the key cells in this process, which can potentially occur in any implant system regardless of implant design or fixation mode. The present study on the effect of nanodiamond particle size on macrophage responses by measuring the proliferation, viability, cellular morphology, apoptosis and phagocytosis (TEM imaging), and genetic expression of pro-inflammatory cytokines and chemokines suggest no potential inflammation due to a size-effect at low concentrations (50–100 μg ml^{-1}) of diamond wear particles. However, the results mandate more studies to evaluate chemotaxis with nanodiamond particles and to evaluate in vivo responses in animal models.

4. Conclusions

Accumulation of wear particles from total joint replacements is a major cause of accelerated prosthetic loosening. To determine the efficacy of the new generation of nanodiamond-coated implants for articulating joint applications, the cellular effects of the incubation of nanodiamonds as possible wear debris with RAW 264.7 cells were investigated. Nanodiamond particles of various sizes (ranging from 6 to 500 nm) were characterized by spectroscopic and microscopic techniques such as XRD, Raman, IR and TEM. Cell proliferation, viability and morphology, as well as the response of genes involved in wear-mediated inflammation, were determined. We observed that cell proliferation, but not metabolic activity, was decreased with nanoparticle sizes of 6–100 nm at low concentration (50 μg ml^{-1}), and both cell proliferation and metabolic activity were significantly reduced at high concentration (200 μg ml^{-1}). Flow cytometry indicated a significant reduction in viable cells irrespective of particle size due to necrosis. qPCR studies showed that nanodiamond exposure significantly reduced gene expression of TNF-α, IL-1β, chemokine Ccl2 and PDGF compared to serum-only controls or anatase (8 nm) nanoparticles, with variable effects on chemokine Cxcl2 and VEGF. TEM images showed evidence of phagocytosis of nanodiamonds.

In short, the present study on the effect of nanodiamond particle size on the macrophage responses by analyses of cell proliferation, cell viability and cell morphology, apoptosis and phagocytosis (TEM imaging), and genetic expression of pro-inflammatory cytokines and

chemokines suggest no potential inflammations due to a size-effect (ranging from 6 to 500 nm) of diamond wear particles at low concentrations (≤50 μg ml^{-1}).

Acknowledgments

We acknowledge support by Award Number R01AR056665 from the National Institute of Arthritis and Musculoskeletal and Skin Diseases. The content is solely the responsibility of the authors and does not necessarily represent the official views of the National Institute of Arthritis and Musculoskeletal and Skin Diseases or the National Institutes of Health. Additional funding from R01 HL092906, NA09OAR4170199 a Research Facilities Improvement Program Grant C06 RR 15490, the Translational Research in Normal and Disordered Development (TReNDD) Program. The authors also wish to thank Mr. Ed Phillips at UAB Microscopy and Imaging Facilities for his help in sample preparation and instrumental support with TEM imaging.

References

1. American Academy of Orthopaedic Surgeons. 2006. <http://www.aaos.org/>
2. Amstutz HC, Campbell P, Kossovsky N, Clarke IC. Mechanism and clinical significance of wear debris induced osteolysis. Clin Orthop Relat Res. 1992; 276:7–18. [PubMed: 1537177]
3. Goldring SR, Schiller AL, Roelke M, Rourke CM, O'Neil DA, Harris WH. The synovial-like membrane at the bone-cement interface in loose total hip replacements and its proposed role in bone lysis. J Bone Joint Surg Am. 1983; 65(5):575–84. [PubMed: 6304106]
4. Mercuri LG. The TMJ concepts patient fitted total temporomandibular joint reconstruction prosthesis in total temporomandibular joint reconstruction. Oral Maxillofac Surg Clin North Am. 2000; 12:73–91.
5. Amstutz HC, Grigoris P. Metal on metal bearings in hip arthroplasty. Clin Orthop Relat Res. 1996; 329:S11–34. [PubMed: 8769320]
6. McKellop H, Park SH, Chiesa R, Doorn P, Lu B, Normand P, et al. In vivo wear of three types of metal on metal hip prostheses during two decades of use. Clin Orthop Relat Res. 1996; 329:S128–40. [PubMed: 8769330]
7. Medley JB, Chan FW, Krygier JJ, Bobyn JD. Comparison of alloys and designs in a hip simulator study of metal on metal implants. Clin Orthop Relat Res. 1996; 329:S148–59. [PubMed: 8769332]
8. Tipper JL, Ingham E, Hailey JL, Besong AA, Fisher J, Wroblewski BM, et al. Quantitative analysis of polyethylene wear debris, wear rate and head damage in retrieved Charnley hip prostheses. J Mater Sci: Mater Med. 2000; 11(2):117–24. [PubMed: 15348056]
9. McGovern TF, Moskal JT. Radiographic evaluation of periprosthetic metallosis after total knee arthroplasty. J South Orthop Assoc. 2002; 11(1):18–24. [PubMed: 12741582]
10. Wagner M, Wagner H. Medium-term results of a modern metal-on-metal system in total hip replacement. Clin Orthop Relat Res. 2000; 379:123–33. [PubMed: 11039799]
11. Hallab N, Merritt K, Jacobs JJ. Metal sensitivity in patients with orthopaedic implants. J Bone Joint Surg Am. 2001; 83(3):428–36. [PubMed: 11263649]
12. Moran CG, Tourret LJ. Recent advances: orthopaedics. BMJ. 2001; 322(7291):902–5. [PubMed: 11302907]
13. Dearnaley G, Arps JH. Biomedical applications of diamond-like carbon (DLC) coatings: a review. Surf Coat Technol. 2005; 200:2518–24.
14. Gutensohn K, Beythien C, Bau J, Fenner T, Grewe P, Koester R, et al. In vitro analyses of diamond-like carbon coated stents—reduction of metal ion release, platelet activation, and thrombogenicity. Thromb Res. 2000; 99(6):577–85. [PubMed: 10974344]
15. Aspenberg P, et al. Benign response to particles of diamond and SiC: bone chamber studies of new joint replacement coating materials in rabbits. Biomaterials. 1996; 17:807–12. [PubMed: 8730965]
16. Chowdhury S, Borham J, Catledge SA, Eberhardt AW, Johnson PS, Vohra YK. Synthesis and mechanical wear studies of ultra smooth nanostructured diamond (USND) coatings deposited by microwave plasma chemical vapor deposition with He/H2/CH4/N2 mixtures. Diamond Relat Mater. 2008; 17:419–24.
17. Catledge SA, Fries MD, Vohra YK, Lacefield WR, Lemons JE, Woodard S, et al. Nanostructured ceramics for biomedical implants. J Nanosci Nanotechnol. 2002; 2:293–312. [PubMed: 12908255]

18. Papo MJ, Catledge SA, Vohra YK, Machado C. Mechanical wear behavior of nanocrystalline and multilayer diamond coatings on temporomandibular joint implants. J Mater Sci: Mater Med. 2004; 15(7):773–7. [PubMed: 15387413]
19. Catledge SA, Vaid R, Diggins P, Weimer JJ, Koopman M, Vohra YK. Improved adhesion of ultra-hard carbon films on cobalt-chromium orthopedic implant alloy. J Mater Sci: Mater Med. 2011; 22:307–16. [PubMed: 21221739]
20. Lappalainen R, Selenius M, Anttila A, Konttinen YT, Santavirta SS. Reduction of wear in total hip replacement prostheses by amorphous diamond coatings. J Biomed Mater Res: Appl Biomater. 2003; 66B:410–3.
21. Alhaddad A, Adam MP, Botsoa J, Dantelle G, Perruchas S, Gacoin T, et al. Nanodiamonds as a vector for siRNA delivery to Ewing sarcoma cells. Small. 201110.1002/smll.201101193
22. Chow EK, Zhang XQ, Chen M, Lam R, Robinson E, Huang H, et al. Nanodiamond therapeutic delivery agents mediate enhanced chemoresistant tumor treatment. Sci Trans Med. 2011; 3:73ra21.10.1126/scitranslmed.3001713
23. Huang H, Pierstorff E, Osawa E, Ho D. Protein-mediated assembly of nanodiamond hydrogels into a biocompatible and biofunctional multilayer nanofilm. ACS Nano. 2008; 2:203–12. [PubMed: 19206620]
24. Weng MF, Chiang SY, Wang NS, Niu H. Fluorescent nanodiamonds for specifically targeted bioimaging: application to the interaction of transferrin with transferrin receptor. Diamond Relat Mater. 2009; 18:587–91.
25. Krueger A. New carbon materials: biological applications of functionalized nanodiamond materials. Chem Eur J. 2008; 14:1382–90. [PubMed: 18033700]
26. Schrand AM, Huang H, Carlson C, Schlanger JJ, Osawa E, Hussain SM, et al. Are diamond nanoparticles cytotoxic. J Phys Chem B. 2007; 111:2–7. [PubMed: 17201422]
27. Burleson T, Yusuf N, Stanishevsky A. Surface modification of nanodiamonds for biomedical application and analysis by infrared spectroscopy. J Ach Mat Manuf Eng. 2009; 37:258–63.
28. Yuan Y, Chen Y, Liu JH, Wang H, Liu Y. Biodistribution and fate of nanodiamonds in vivo. Diamond Relat Mater. 2009; 18(1):95–100.
29. Maloney WJ, Smith RL. Periprosthetic osteolysis in total hip arthroplasty: the role of particulate wear debris. J Bone Joint Surg Am. 1995; 77:1448–61.
30. Bauer TW. Particles and periimplant bone resorption. Clin Orthop Relat Res. 2002; 405:138–43. [PubMed: 12461365]
31. Wang ML, Sharkey PF, Tuan RS. Particle bioreactivity and wear mediated osteolysis. J Arthroplasty. 2004; 19:1028–38. [PubMed: 15586339]
32. Purdue PE, Koulouvaris P, Potter HG, Nestor BJ, Sculco TP. The cellular and molecular biology of periprosthetic osteolysis. Clin Orthop Relat Res. 2007; 454:251–61. [PubMed: 16980902]
33. Ingham E, Fisher J. The role of macrophages in osteolysis of total joint replacement. Biomaterials. 2005; 26:1271–86. [PubMed: 15475057]
34. Glant TT, Jacobs JJ, Molná RG, Shanbhag AS, Valyon M, Galante JO. Bone resorption activity of particulate-stimulated macrophages. J Bone Miner Res. 1993; 8:1071–9. [PubMed: 8237476]
35. Merkel KD, Erdmann JM, McHugh KP, Abu-Amer Y, Ross FP, Teitelbaum SL. Tumor necrosis factor-a mediates orthopedic implant osteolysis. Am J Pathol. 1999; 154:203–10. [PubMed: 9916934]
36. Hill MR, Catledge SA, Konovalov V, Clem WC, Chowdhury SA, Etheridge BS, et al. Preliminary tribological evaluation of nanostructured diamond coatings against ultra-high molecular weight polyethylene. J Biomed Mater Res: Appl Biomater. 2008; 85B:140–8.
37. Tipper JL, Firkins PJ, Besong AA, Barbour PSM, Nevelos J, Stone NH, et al. Characterization of wear debris from UHMWPE on zirconia ceramic, metal-on-metal and alumina ceramic-on-ceramic hip prostheses generated in a physiological anatomical hip joint simulator. Wear. 2001; 250:120–8.
38. Kong XL, Huang CL, Hsu CM, Chen WH, Han CC, Chang HC. High-affinity capture of proteins by diamond nanoparticles for mass spectrometric analysis. Anal Chem. 2005; 77:259–65. [PubMed: 15623304]

39. Bailey LO, Lippiatt S, Biancanello FS, Ridder SD, Washburn NR. The quantification of cellular viability and inflammatory response to stainless steel alloys. Biomaterials. 2005; 26:5296–302. [PubMed: 15814127]
40. Chomczynski P, Sacchi N. Single-step method of RNA isolation by acid guanidinium thiocyanate-phenol-chloroform extraction. Anal Biochem. 1987; 162:156–9. [PubMed: 2440339]
41. James ML, Ross AC, Bulger A, Philips J, Ambalavanan N. Vitamin A and eetinoic acid act synergistically to increase lung retinyl esters during normoxia and reduce hyperoxic lung injury in newborn mice. Pediactric Res. 2010; 67:591–7.
42. Chang IP, Hwang KC, Ho JA, Lin CC, Hwu RJR, Horng JC. Facile surface functionalization of nanodiamonds. Langmuir. 2010; 26(5):3685–9. [PubMed: 19856970]
43. Xia Z, Triffitt JT. A review on macrophage responses to biomaterials. Biomed Mater. 2006; 1:R1–9. [PubMed: 18458376]
44. Schwarz EM, Lu AP, Goater JJ, Benz EB, Kollias G, Rosier RN, et al. Tumor necrosis factor-alpha/nuclear transcription factor-κB signaling in periprosthetic osteolysis. J Orthop Res. 2000; 18:472–80. [PubMed: 10937636]
45. Algan SM, Purdon M, Horowitz SM. Role of tumor necrosis factor alpha in particulate-induced bone resorption. J Orthop Res. 1996; 14:30–5. [PubMed: 8618163]
46. Goodman SB, Ma T. Cellular chemotaxis induced by wear particles from joint replacements. Biomaterials. 2010; 31:5045–50. [PubMed: 20398931]
47. Epstein NJ, Bragg WE, Ma T, Spanogle J, Smith RL, Goodman SB. UHMWPE wear debris upregulates mononuclear cell proinflammatory gene expression in a novel murine model of intramedullary particle disease. Acta Orthopaedica. 2005; 76(3):412–20. [PubMed: 16156472]
48. Brodbeck WG, Shive MS, Colton E, Ziats NP, Anderson JM. Interleukin-4 inhibits tumor necrosis factor-alpha-induced and spontaneous apoptosis of biomaterial-adherent macrophages. J Lab Clin Med. 2002; 139:90–100. [PubMed: 11919547]
49. Kyriakides TR, Foster MJ, Keeney JE, Tsai A, Giachelli CM, Clark-Lewis I, et al. The CC chemokine ligand, CCL2/MCP1, participates in macrophage fusion and foreign body giant cell formation. Am J Pathol. 2004; 165:2157–66. [PubMed: 15579457]
50. Xu JW, Konttinen YT, Li TF, Waris V, Lassus J, Matucci-Cerinic M, et al. Production of platelet-derived growth factor in aseptic loosening of total hip replacement. Rheumatol Int. 1998; 17:215–21. [PubMed: 9592860]
51. Pipino F. The bone-prosthesis interaction. J Orthop Traumatol. 2000; 1:3–9.
52. Zhang W, Peng X, Cheng T, Zhang X. Vascular endothelial growth factor gene silencing suppresses wear debris induced inflammation. Int Orthop. 201110.1007/s00264-011-1252-4
53. Konovalov VV, Melo A, Catledge SA, Chowdhury S, Vohra YK. Ultra-smooth nanostructured diamond films deposited from He/H2/CH4/N2 microwave plasmas. J Nanosci Nanotechnol. 2006; 6(1):258–61. [PubMed: 16573106]
54. Chowdhury S, Catledge SA, Konovalov VV, Vohra YK. Synthesis of ultrasmooth nanostructured diamond films by microwave plasma chemical vapor deposition using a He/H2/CH4/N2 gas mixture. J Mater Res. 2006; 21(10):2675–82. [PubMed: 18946515]
55. Catledge SA, Thomas V, Vohra YK. Effect of surface oxides and intermetallics on nanostructured diamond coating of nitinol for stent applications. Curr Nanosci. 2006; 2:9–12.
56. Bhushan B. Chemical, mechanical and tribological characterization of ultra-thin and hard amorphous carbon coatings as thin as 3.5 nm: recent developments. Diamond Relat Mater. 1999; 8:1985–2015.
57. Catledge, SA.; Vohra, YK. Nanostructured surface modifications for biomedical implants. In: Nalwa, HS., editor. Encyclopedia of nanoscience and nanotechnology. Valencia, CA: American Scientific Publishers; 2004. p. 741-62.
58. Clem WC, Chowdhury S, Catledge SA, Weimer JJ, Shaikh FM, Hennessy KM, et al. Mesenchymal stem cell interaction with ultra-smooth nanostructured diamond for wear-resistant orthopaedic implants. Biomaterials. 2008; 29:3461–8. [PubMed: 18490051]
59. Revell PA. The combined role of wear particles, macrophages and lymphocytes in the loosening of total joint prostheses. J R Soc Interface. 2008; 5:1263–78. [PubMed: 18647740]

Appendix A. Figures with essential colour discrimination

Certain figures in this article, particularly Figures 1 and 2, are difficult to interpret in black and white. The full colour images can be found in the on-line version, at doi:10.1016/j.actbio.2012.01.033.

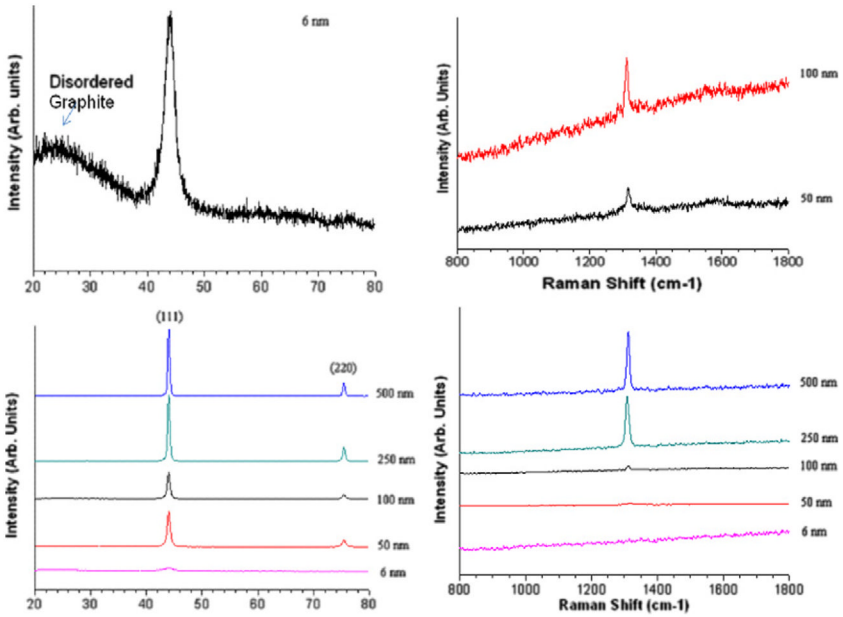

Fig. 1.
XRD and Raman spectral characterization of different nanodiamond particles.

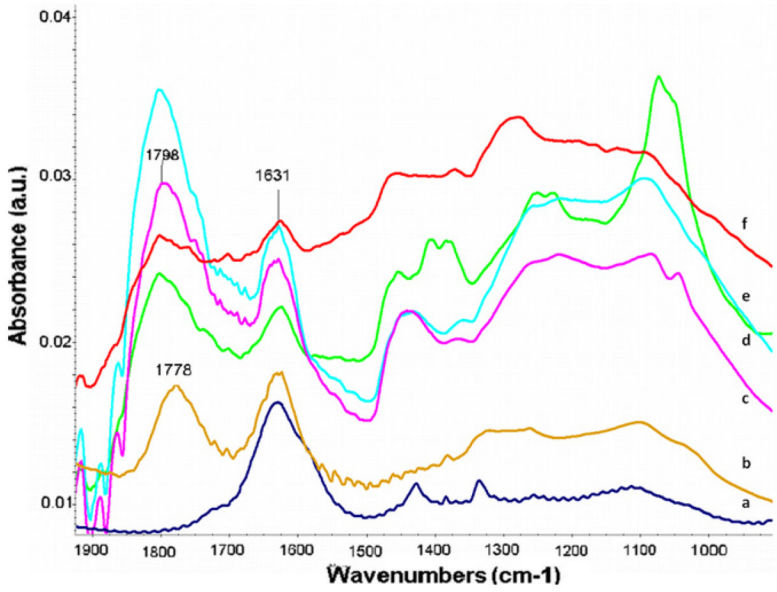

Fig. 2.

FT-IR spectral characterization of different nanodiamond particles: 6 nm nanodiamond before (a) and after (b) acid treatment indicating appearance of peak for –COOH group; (c–f) respectively 60, 100, 250 and 500 nm diamond after acid treatment.

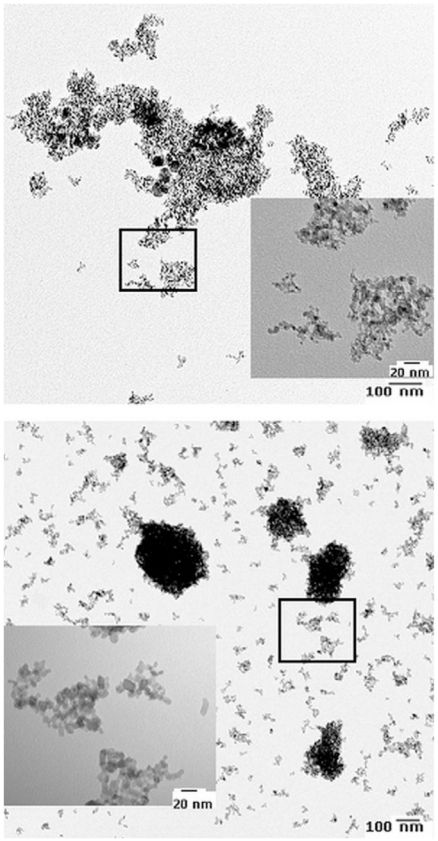

Fig. 3.
Representative TEM photomicrographs of ~6 nm nanodiamonds and ~8 nm TiO_2 nanoparticles dispersed in PBS.

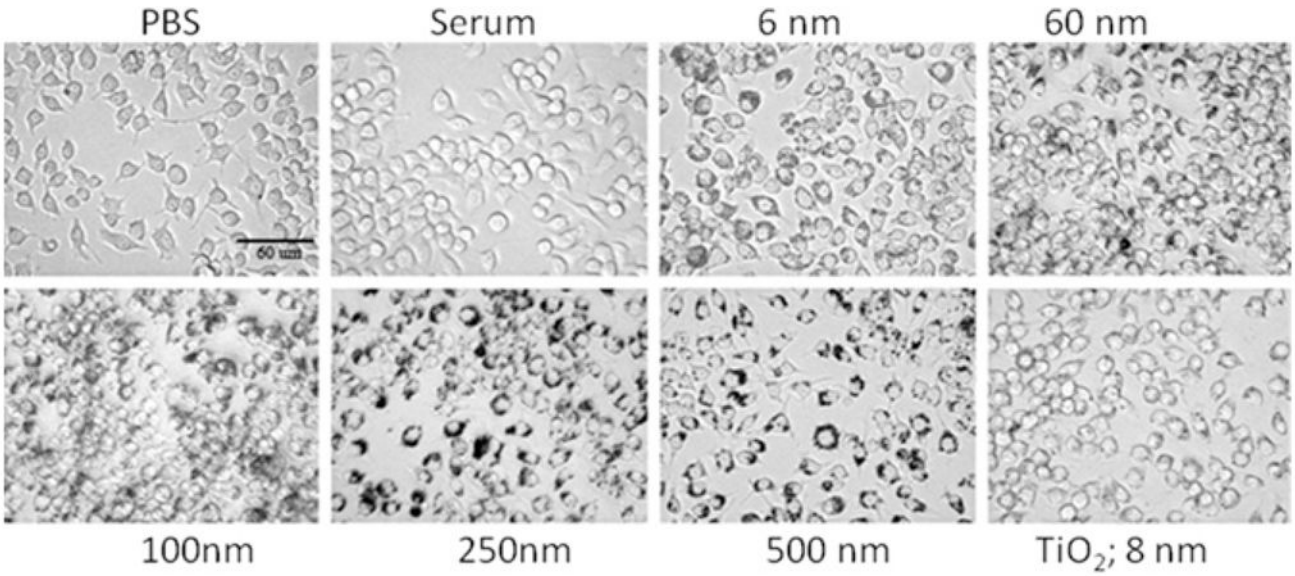

Fig. 4.

Photomicrographs (400×) showing the morphology of Raw 264.7 cells cultured in the presence of nanodiamonds of various sizes (6–500 nm) and TiO_2 nanoparticles (50 μg ml^{-1}) in comparison with cells cultured in PBS and human serum (controls). Scale bar = 60 μm.

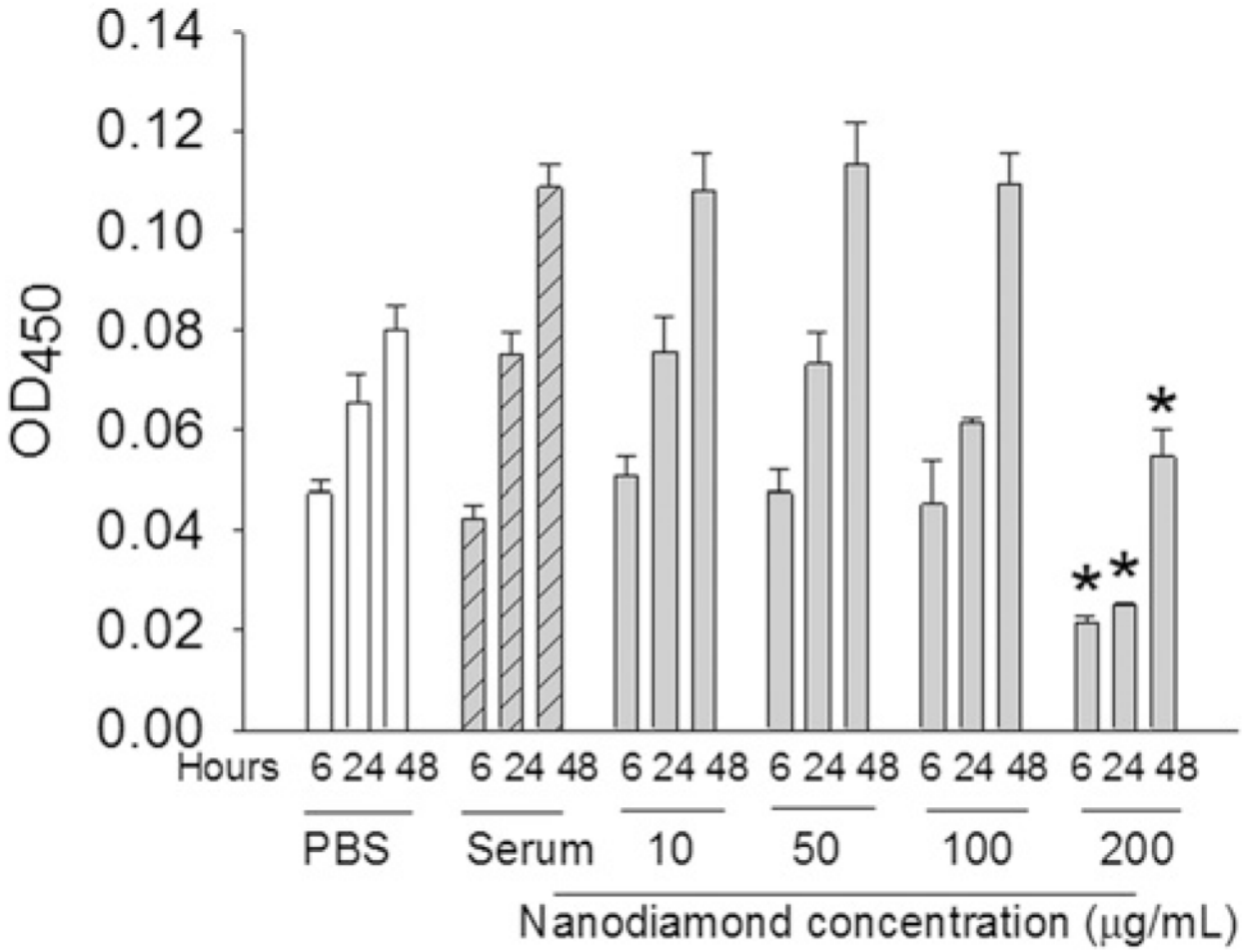

Fig. 5.

Effect of concentration of 6 nm nanodiamonds on cell metabolic activity measured by WST-1 assay after culturing the cells (~40,000 Raw 264.7 cells per well) in the presence of varying concentrations of nanodiamonds (10–200 μg ml^{-1}) for 24 h. *$P < 0.05$ vs. other concentrations at same time point.

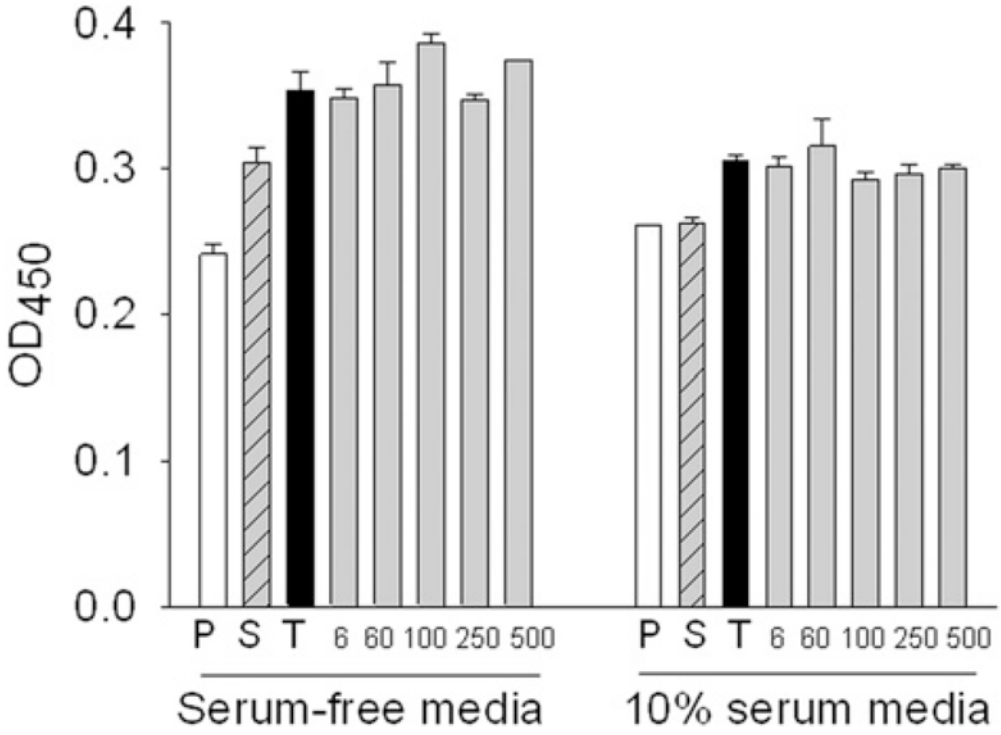

Fig. 6.

Effect of human serum incubated nanodiamonds at 50 μg ml^{-1} for 24 h on cell metabolic activity by WST-1 assay. P = PBS; S = Serum; T = TiO_2 NP; 6, 60, 100, 250, 500 are sizes of nanodiamonds in nm. All nanoparticles (both titanium dioxide and nanodiamond) significantly differ from PBS and serum.

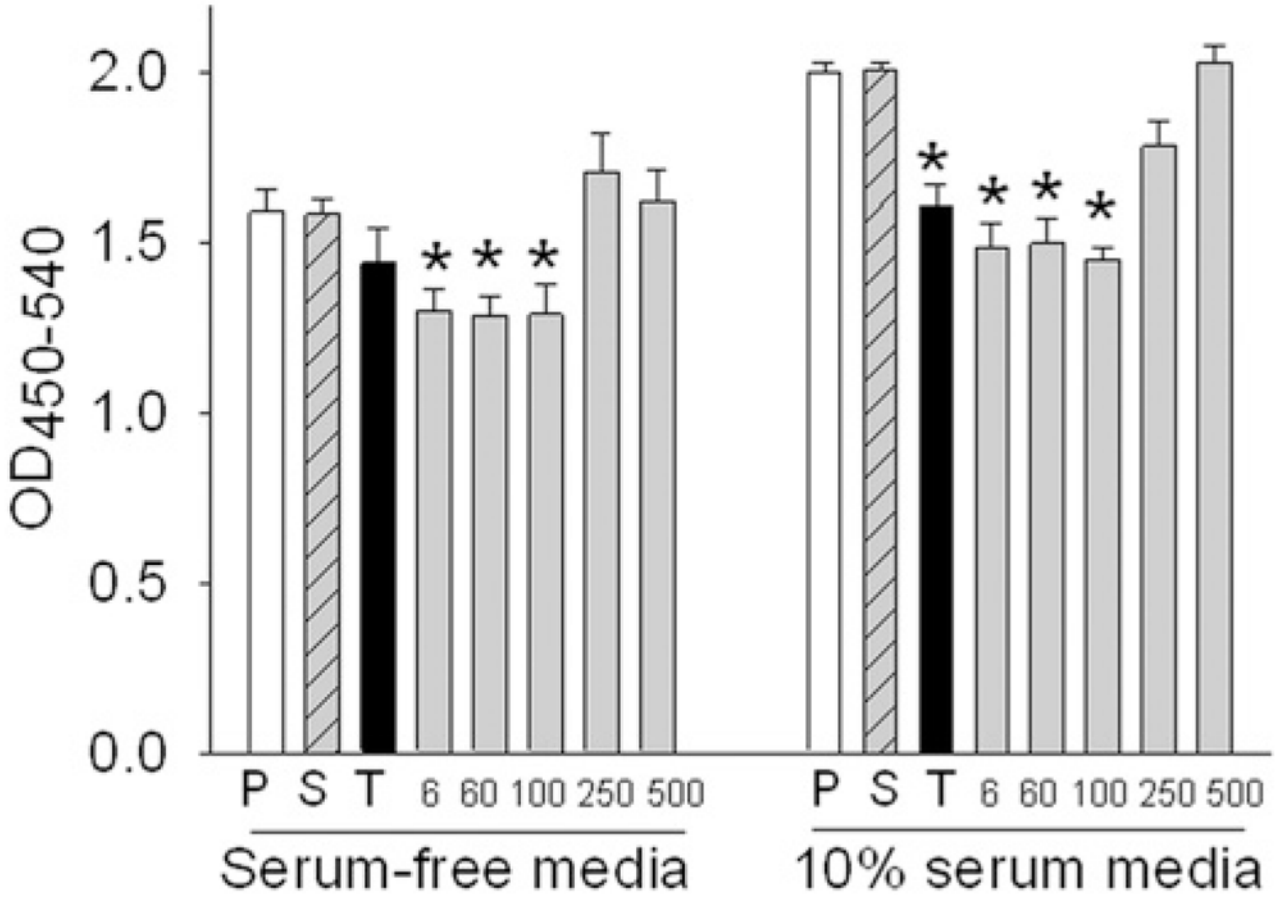

Fig. 7.

Effect of human serum incubated nanodiamonds at 50 μg ml^{-1} for 24 h on cell proliferation by BrdU immunoassay. P = PBS; S = Serum; T = TiO_2 NP; 6, 60, 100, 250, 500 are sizes of nanodiamonds in nm. *$P < 0.05$ vs. corresponding serum-only (S) or PBS (P) control.

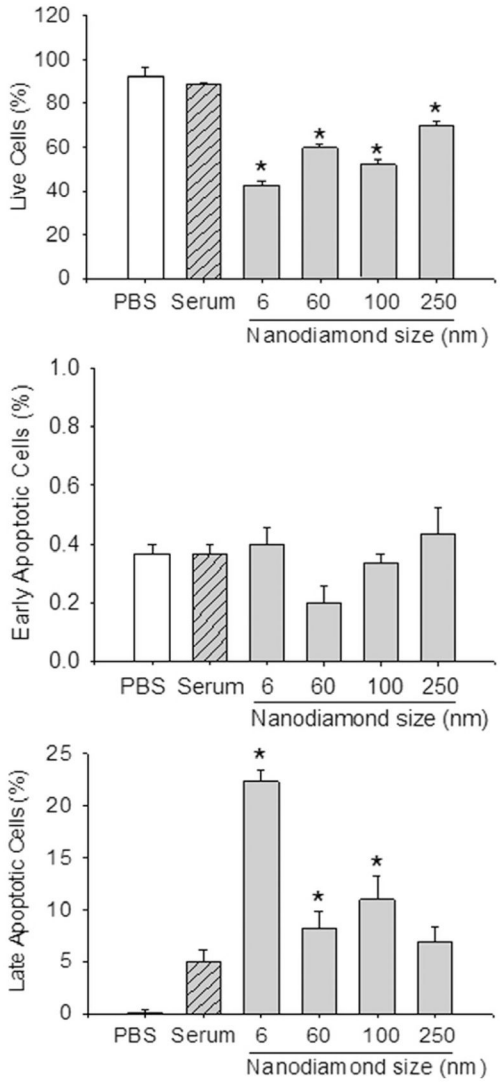

Fig. 8.

Apoptosis and cell viability as estimated by flow cytometry after culturing. 200,000 cells per well with 50 μg ml^{-1} nanodiamonds in MEM containing 10% FCS were cultured for 24 h on a 24-well plate. After washing with 250 μl PBS, cells were labeled with propidium iodide and Annexin V-FITC (1:100). Among the apoptotic dye-positive cells, Annexin V-FITC labeled cells were plotted as early apoptotic cells and propidium iodide + Annexin-V-FITC labeled cells were plotted as late apoptotic cells. Unlabeled (non-apoptotic) cells were plotted for cell viability. *$P < 0.05$ vs. serum-only or PBS control.

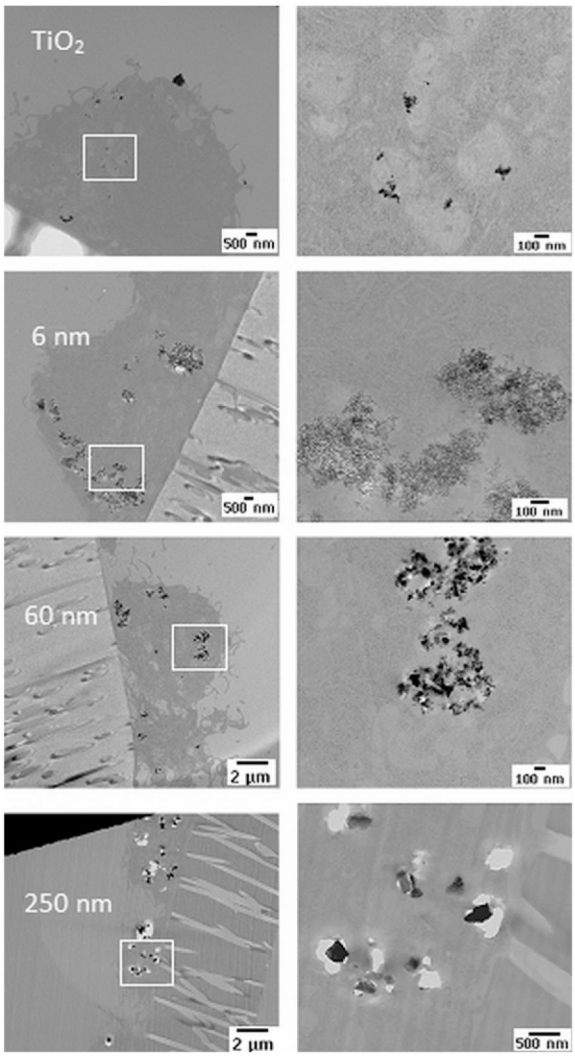

Fig. 9.
TEM images showing the internalization of TiO_2 nanoparticles (~8 nm) and nanodiamond particles (6, 60 and 250 nm). Higher-magnification images of the corresponding marked area are given on the right side of each image.

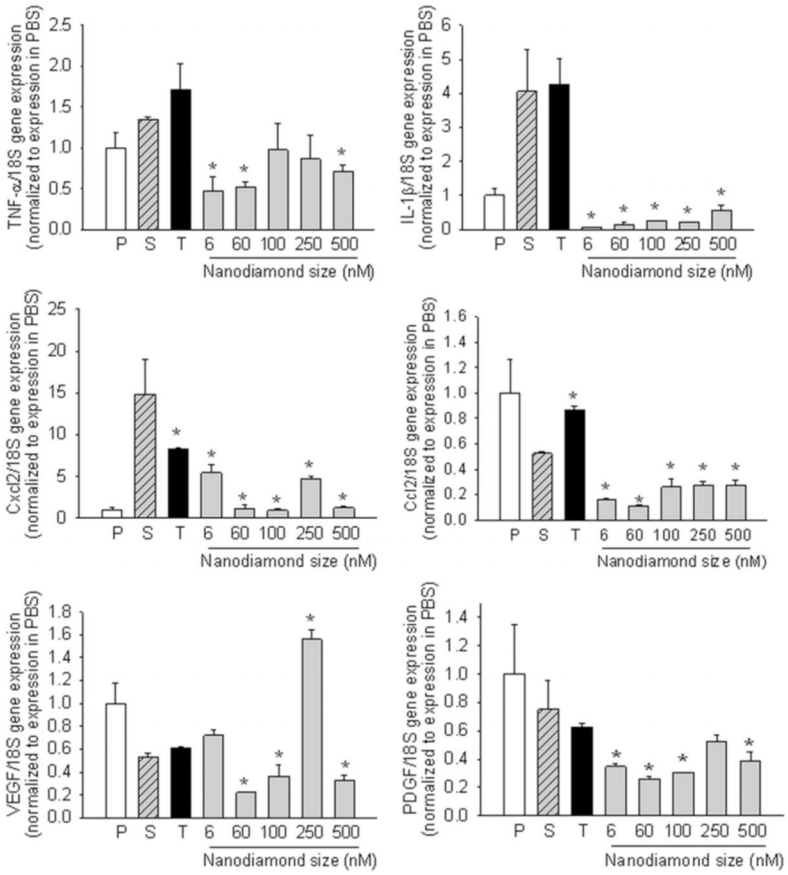

Fig. 10.

Gene expression of selected cytokines and growth factors. P = PBS; S = Serum; T = TiO_2 NP; **P* < 0.05 vs. serum control.

Table 1

Mouse primer sequences for real-time quantitative PCR.

Primer name and orientation	Sequence
18S forward	CTT-AGT-TGG-TGG-AGC-GAT-TTG
18S reverse	GCA-ATA-ACT-GGT-CTG-TGA-TG
ACTB forward	TTG-CTG-ACA-GGA-TGC-AGA-AG
ACTB reverse	CAA-GCA-GGA-GTA-CGA-TGA-GTC
TNF-α forward	TTC-GAG-TGA-CAA-GCC-TGT-AG
TNF-α reverse	CTA-CAT-GGA-TGA-AAC-CTC-TT
IL-1β forward	ACT-GTG-AAA-TGC-CAC-CTT-TTG
IL-1β reverse	CAG-TAT-CAC-TCA-TTG-TGG-CT
Cxcl2 forward	CCA-CTC-TCA-AGG-GCG-GTC-AAA
Cxcl2 reverse	TAC-GAT-CCA-GGC-TTC-CCG-GGT
PDGFA forward	TAA-CAC-CAG CAG CGT CAA GTG
PDGFA reverse	CTG-GAC-CTC-TTT-CAA-TTT-TGG-C
VEGFA forward	GAG-CGG-AGA-AAG-CAT-TTG-TTT-G
VEGFA reverse	CGT-TCG-TTT-AAC-TCA-AGC-TGC-C
Ccl2 forward	AGG-TCC-CTG-TCA-TGC-TTC-TGG
Ccl2 reverse	GTG-AAT-GAG-TAG-CAG-CAG-GTG-AG